Synthetic Nervous System Control of a Bioinspired Soft Grasper for Pick-and-Place Manipulation*

Ravesh Sukhnandan[1+], Yanjun Li[4+], Yu Wang[1], Anaya Bhammar[1], Kevin Dai[1], Michael Bennington[1], Hillel J. Chiel[5,6,7], Roger D. Quinn[4], and Victoria A. Webster-Wood[1,2,3]

[1]Dept. of Mechanical Engineering, [2]Dept. of Biomedical Engineering,
[3]McGowan Institute for Regenerative Medicine
Carnegie Mellon University, Pittsburgh, PA, United States

[4]Department of Mechanical Engineering, [5]Department of Biology,
[6]Department of Neurosciences,[7]Department of Biomedical Engineering
Case Western Reserve University, Cleveland, OH, United States

[+]These authors contributed equally to the work.
vwebster@andrew.cmu.edu

Abstract. Manipulation of objects of variable size, shape and surface properties remains a challenging problem in robotics. In this paper, we present the design of a soft, pneumatically variable contact stiffness grasper and the training of a sparse, bioinspired neural network controller for pick-and-place manipulation. Both the soft grasper and the neural network controller are inspired by the sea slug *Aplysia californica*. The compliant nature of the grasper is beneficial for maintaining rich contact with objects, which simplifies the control problem. Adopting biologically inspired neural dynamics and network structure has the further advantage of building neural network controllers that are robust and efficient for real-time control. To verify the effectiveness of our bio-inspired approach for object grasping and manipulation, we developed a simulation environment that reflects the compliance between the soft grasper and the object. We demonstrate that when integrated with the neural network controller, the grasper successfully completed the pick-and-place task in simulation. With minimal tuning, the controller was then successfully transferred to the physical soft grasping platform and was able to successfully pick-and-place objects of various size and mass, up to a maximum tested mass of 706 g. The bio-inspired approach to both the morphology and the control of the soft-grasper presented here thus represents an exciting first step toward the robust adaptive manipulation of a broad class of objects.

* This work was supported in part by the National Science Foundation (NSF) grant no. FRR-2138873 and by a GEM fellowship. Any opinions, findings, and conclusions or recommendations expressed in this material are those of the authors and do not necessarily reflect the views of the NSF.

Keywords: Soft robotics · Robotic Manipulation · Synthetic Nervous Systems · *Aplysia*.

1 Introduction

In the pursuit of robotic manipulators that can replicate the dexterity and sensitivity of prehensile appendages found in nature, roboticists have increasingly incorporated soft materials and compliant structures in their designs [1, 21, 27]. Soft graspers offer advantages that make them attractive options for the manipulation of objects in challenging environments, such as in agriculture. Some fruit, fungi, and vegetables are often soft, slippery, and fragile [37]. Soft graspers and compliant structures can solve contact problems encountered in the manipulation of such objects morphologically by conforming to the surface of the object [27]. Moreover, unlike point contact between rigid bodies, compliant structures have the ability to conform to the grasped object, which increases the contact area and the frictional forces and torques that can be applied to keep the object stable [2].

Prehensile appendages like tentacles [1] and soft fingertips [22] often serve as a direct source of inspiration for the morphology of their soft robotic counterparts [27]. However, soft structures possess many degrees of freedom, which make predicting how these structures will deform computationally expensive. The computational cost is further compounded when the objects being grasped are soft or irregular. Hence, the real-time control of soft robotic grasping and manipulation systems remains a challenge [33]. However, many natural organisms are capable of similar real-time control to execute such complicated manipulation tasks.

One organism that is adept at grasping and manipulating a wide variety of objects, including small, fragile, and slippery objects in real-world settings using a soft grasper is the sea slug *Aplysia californica*. *Aplysia* regularly manipulates seaweeds of a wide range of geometries and stiffness and adapts to mechanical loads in the environment. Furthermore, *Aplysia* possesses a tractable nervous system that has facilitated the creation of detailed neuromechanical models of its soft grasper and neural controller [34]. This detailed understanding of both the biomechanics and neural controller of *Aplysia* has been used to create soft robots that can capture the major kinematics of *Aplysia*'s feeding behavior [5,21]. Abstracting key features from *Aplysia*'s feeding mechanisms for engineering applications may help to bridge the gap between the manipulation benefits inherent to soft graspers and the difficulty in controlling such structures.

Adapting the advantages of *Aplysia*'s soft grasper for engineering applications requires the adoption of principles from both the grasper's morphology and control. *Aplysia*'s soft grasper can conform to the shape of a grasped object by enveloping it within the soft grasper and modulating the shape of its lumen [14]. Through active modulation of closing force in the musculature of the grasper [10], it can tune the contact stiffness of the grasper to maintain a secure hold of the object. To mimic the modulatory characteristics of the

Aplysia grasper in soft robots, a combination of grasper morphology and material properties can be exploited to achieve tunable stiffness. Methods to modulate contact stiffness through thermally actuated polymers and metals [3, 24], dielectric elastomers (DEA) [28] and dielectric liquids [36], and variable fluidic pressure [16, 22, 29] have previously been used by soft roboticists, but gaps remain. For example, thermally actuated methods can achieve order of magnitude changes in stiffness but can require timescales on the order of minutes to do so [24]. Dielectric elastomer and dielectric liquid based graspers have the advantage of direct interfacing with electrical control systems. However, they require operating voltages on the order of kilovolts (kV) [28,36] which needs specialized circuitry and handling [20]. Fluidic actuated graspers can achieve tunable stiffness by modulating pressure, while simultaneously providing feedback of contact pressure [22] and geometry [16, 29]. The graspers presented in [16, 29] and [22] achieve tunable stiffness with feedback of contact by modulating and monitoring pressure in an elastic enclosure. However, these graspers adopt a parallel jaw configuration which limits their ability to spatially tune stiffness and maximize the surface area in contact with the target object. Although other fluidic graspers have been reported that can provide a greater contact area with the object using stochastic tentacle-like appendages [1] or a fluidic toroid [25], they do not explicitly provide the ability to spatially tune contact stiffness and sense changes in contact state along the grasping surface.

In addition to the compliance and tunable materials of *Aplysia*'s feeding apparatus, the controller for *Aplysia*'s soft grasper demonstrates real-time control of feeding behavior that adapts to the environment. The controller exhibits a hierarchical control architecture that is composed of command and interneurons that creates emergent adaptability based on sensory feedback [34]. To create a similar, real-time controller for our *Aplysia*-inspired soft grasper, we implemented a Synthetic Nervous System (SNS) controller. SNSs incorporate the dynamics of real neurons and can be designed to perform basic arithmetic operations efficiently, which makes them a promising approach for the control of real-time robotic systems [9, 31, 32]. Furthermore, SNSs can be designed to replicate a hierarchical control architecture, inspired by that found in *Aplysia* [18]. We have previously demonstrated that an SNS tuned in simulation can successfully control a Cartesian gantry robot for a real-time pick-and-place manipulation task [18]. However, SNSs have not been previously used to control a soft grasper in a manipulation task. SNSs' ability to robustly and efficiently perform computations in real-time [18] makes it particularly attractive for the real-time control of a soft grasper for manipulating objects of various sizes, shapes, and surface properties.

To address the need for real-time control of soft robotic graspers for pick-and-place manipulation, in this work, we present the design, manufacturing, and characterization of a bio-inspired soft grasper based on the abstraction of key features from the feeding mechanism of *Aplysia californica*. The grasper's morphology was inspired by the conformable grasping surface of *Aplysia*, and was able to envelop grasped objects via pneumatic soft actuators that contract

radially. Spatial tuning of contact stiffness was achieved by soft jaws with pneumatically variable contact stiffness, which also simultaneously provide contact feedback via monitoring of abrupt pressure changes. We then show that an SNS controller inspired by the hierarchical structure of the *Aplysia* feeding control circuitry can be first tuned in simulation and then transferred to the physical soft robotic grasper to perform pick-and-place manipulation, with limited additional tuning. The physical grasper qualitatively replicated the key dynamics of the simulated grasper. Without any additional tuning of the controller, the soft grasper with SNS control was able to pick up objects of varying size, shape, and mass. This work lays the foundation for a soft grasper platform that can adaptively change its control and actuation to robustly manipulate objects of various shape and surface properties. Such a grasping platform may be particularly useful in an agricultural environment where the ability to simultaneously modulate and sense contact pressure can aid in the manipulation of soft, fragile, and slippery objects.

2 Methods

2.1 Bioinspired Soft Grasper

Assembly and Characterization of Closure Artificial Muscle. To achieve circumferential contraction of the closure muscle, two layers of McKibben actuators are placed in a fabric sleeve (80% Nylon, 20% Spandex). Each layer of actuators was composed of two McKibben actuators fabricated using methods previously described by Dai et al. [5], each 245 mm long, connected via 1.6 mm (1/16 in.) inner diameter (ID) tubing. To maintain a cylindrical shape, the layers of McKibbens were offset by 90 degrees (Fig. 1A). This 90-degree offset minimized the strain on the tubing connections between the McKibben actuators, which otherwise had a tendency to buckle when pressurized. This buckling would cause the closure muscle to lose its circular shape if only one actuator layer was used.

When actuated, these McKibben's exhibited approximately 25% contraction from their original length. For a closure muscle of circumferential length of 490 mm, we would expect to see a change of radius of the circular area of the actuator from 46.5 mm when fully deflated to 19.5 mm when fully inflated, for a total radial change of 27 mm (Fig. 1A). To characterize the contraction of the fabricated closure muscle, the pressure applied to the muscle was increased from 0 to 12 psig at increasing intervals of 0.5 psig. At every pressure point, the system was pneumatically inflated in a twenty-second period, and three measurements of the diameter of the muscle were taken on the inner wall of the closure muscle with a 1-mm resolution ruler.

Assembly and Characterization of Soft Jaws with Tunable Stiffness. While the closure muscle became increasingly stiff with applied pressure, this change was coupled with a decrease in diameter. Moreover, it was not possible

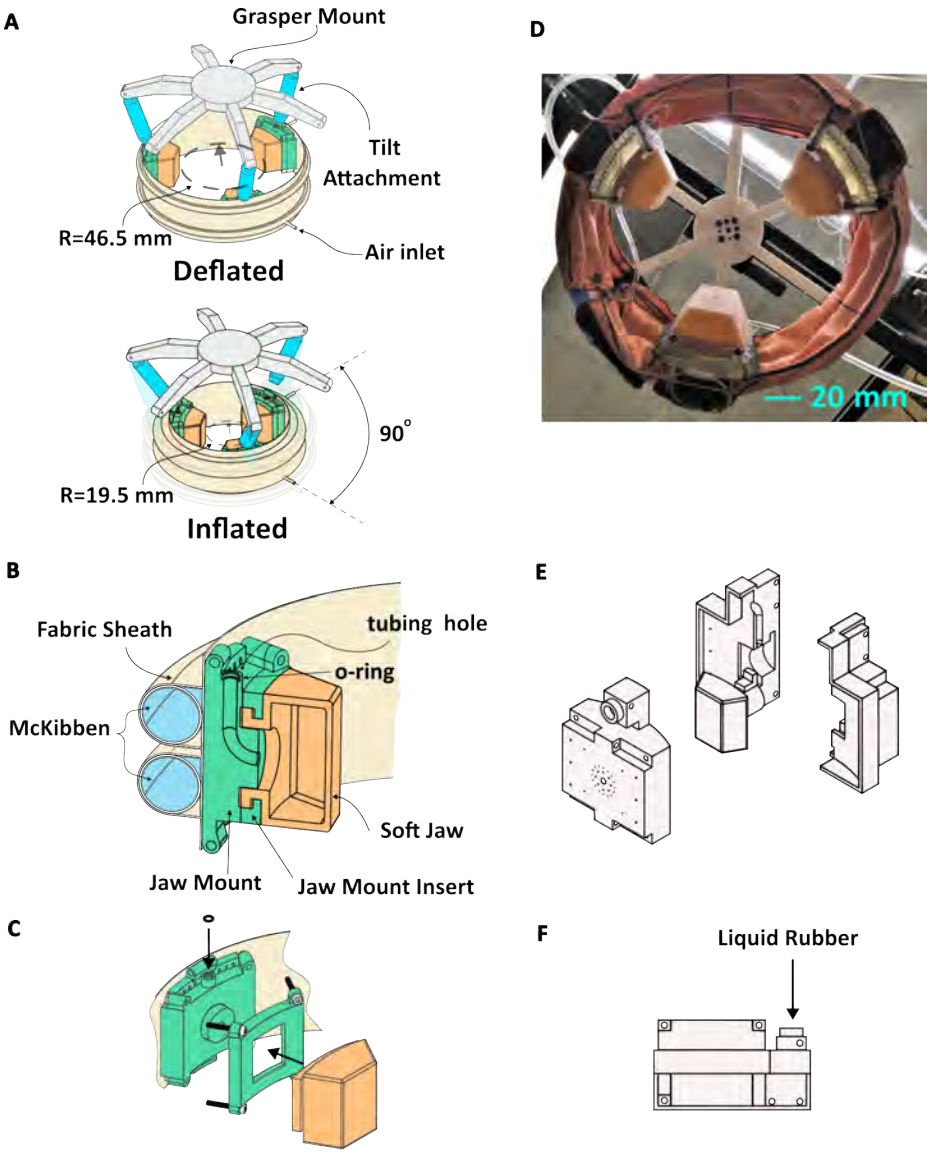

Fig. 1. A. Schematic of grasper in the uninflated and inflated states. **B** Cross-section of the soft grasper. Air tightness was kept via the flange of the soft jaw. **C** Exploded view of soft jaw assembly. **D** Fabricated Grasper (underside view). The soft grasper without the tilt attachments weighed 143 g. The total radial contraction of the manufactured grasper was 19 mm. **E** Mold used to create the soft jaw. **F** After the mold was assembled, the liquid urethane elastomer was injected via a syringe.

to spatially tune the contact stiffness of the closure actuator. To be able to tune the contact stiffness spatially and to decouple the contact stiffness from the positional state of the closure muscle, soft deformable jaws were designed and affixed to the inner diameter of the closure muscle (Fig. 1). The stiffness of these jaws could be varied pneumatically, such that increasing the air pressure to the internal cavity of a jaw increased its effective stiffness.

To fabricate the jaws, an injection molding technique was used. A four-piece mold was 3D printed on a Prusa MK3S+ out of Hatchbox PRO+ polylactic acid filament (PLA) and sprayed with mold release (Mann). Then, a liquid urethane rubber was mixed according to the manufacturer's instructions (Smooth-On Vytaflex 30A) and was placed in a vacuum chamber @ -100 kPa for 20 minutes to remove bubbles introduced during mixing. The four-piece mold was then assembled (Fig. 1E), and the liquid rubber was injected into the inlet with a syringe (Fig. 1F). The liquid rubber was left for 24 hours at room temperature to cure. After curing, the mold was disassembled, and the soft jaw was removed from the core. Smooth-on Vytaflex 30A was chosen in part because of its ability to withstand up to 1000% strain, which facilitates not only high deformations during grasping but also removal from the mold during fabrication.

To enable a modular design where soft jaws of different sizes, geometries, and material properties could be used, the jaw mounts were attached to the soft grasper, and a removable attachment insert was used to fasten the flange of the soft jaws to the jaw mount using four M2 screws. The mount and insert were 3D printed on an Asiga Freeform PICO2 using a 79D shore hardness resin (PlasCLEAR) with 0.1 mm layer height. The mount included routing channels for the air inlet, which was attached to the pressure controller with a 3.2 mm (1/8 in.) outer diameter (OD) and 1.6 mm (1/16 in.) inner diameter (ID) tube. To ensure air-tightness between the mount and the air inlet, a 4.5 mm OD, 2.5 mm ID, 1 mm thick rubber O-ring (McMaster-Carr) was placed in a slot in the inlet tube pathway. The flange of the soft jaw was slightly oversized for the cavity formed between the mount and the insert (Fig. 1 B-C), which aided in making an airtight seal when tightened with the M2 screws. To further prevent air leaks at the boundary of the soft jaw and the jaw mount, Loctite SI5011 Silicone RTV sealant was applied around the boundary before final assembly.

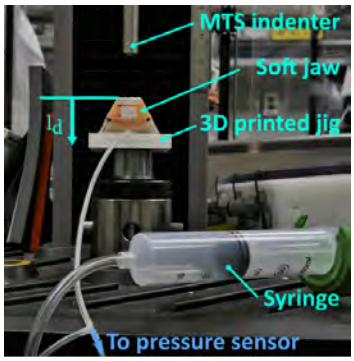

Fig. 2. Experimental setup to characterize the soft jaw stiffness as a function of indentation depth and pressure.

To characterize the stiffness of the jaws, the soft jaw and mount assembly were placed in a 3D printed jig on an MTS Criterion 42 electromechanical load testing system (Fig. 2). A syringe was connected to the air inlet of the jaw, with a 30 psig pressure gauge (ELVH-030G-HAND-C-PSA4) used to monitor the pressure. To achieve a given pressure setpoint, a caulking gun (Albion B12 26:1) was used

to actuate the syringe and hold it in place. Then, the MTS indenter (diameter 12.7 mm) was lowered at a speed of 2 mm/s up to a maximum indentation depth of 5 mm. Pressure setpoints of 0, 0.1, 0.2, 0.3, 0.4, 0.5, 0.6, 0.7, 1.0, 1.5, 1.8, and 2.5 psig were tested, with each setpoint experiment repeated three times. The zero indentation depth for all pressure setpoints was set at the height of the soft jaw when it was uninflated, i.e. the pressure was 0 psig. An empirical model of the measured reaction force as a function of indentation depth and the applied pressure was then fitted for use in the simulation of the soft grasper.

Assembly of Complete Soft Grasper. To assemble the complete soft grasper for pick-and-place manipulation, the soft jaws were first connected to the closure muscle via hook-and-loop fasteners and secured in place via stitches with Kevlar thread through inserts placed in the jaw holder. This was necessary to prevent the jaws from tilting around the closure muscle when it attempted to lift objects. Rigid graspers with only two frictional contact points with the grasped objects often cannot resist moments about the axis that join the contacts [19]. A minimum of three contact points greatly improves the ability to resist external forces and torques applied to the grasped object and establish force closure [19]. To improve the stability of the grasped object, three soft jaws were attached to the closure muscle spaced 120^o apart. Note that the design could accommodate a total of 6 jaws spaced 60^o apart if there is a need for greater contact force or finer tuning of spatial stiffness. The soft grasper was then connected to a gantry via a 3D printed mount, with 3D printed tilt attachments that rotate to allow the closure muscle to contract and relax (Fig. 1A). The gantry was built using a Creality CR-10 S5 3D printer whose firmware was modified to accept M-code commands to control the grasper's position and report its current positional state [18].

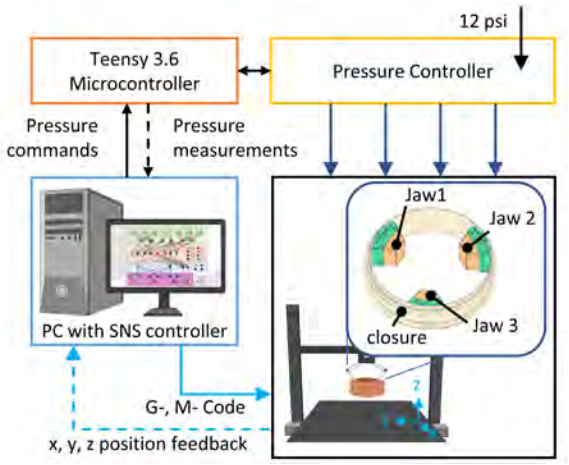

Fig. 3. Block diagram of the robotic system to demonstrate real-time control of the soft grasper for a pick-and-place task. Geometry (G-) and Machine (M-) Code which contains the position commands for the gantry are used to communicate between the computer and the gantry. PC Icon from Biorender.com.

2.2 Simulation Environment

To facilitate the design of a controller for real-time pick-and-place tasks in the soft grasper, a simulation of the soft grasper's mechanics was implemented in

PyBullet (Fig. 7) [4]. The simulation uses a gantry system for spatial positioning of the grasper as described in our prior work [18]. The mechanics of the closure muscle were simulated as linear motor-powered prismatic joints along which each jaw can slide. To take advantage of PyBullet's fast computation for rapid controller tuning, the soft jaws were represented as rigid bodies with a contact stiffness that varied with applied pressure in accordance with the experimentally characterized soft jaw stiffness. To simulate a pick-and-place task, a 1kg cube of size (39, 39, 34.5) mm was placed at the initial position ([0, 0, -0.315] m). The target position for the pick-and-place operation was [0.15, 0.15, -0.335] m. The coefficient of friction between the object and the soft grasper was set as 0.75, which is a typical value of the static coefficient of friction between rubber and other materials [26]. Note that the target position $(x_\mathrm{t}, y_\mathrm{t}, z_\mathrm{t})$ and object position $(x_\mathrm{o}, y_\mathrm{o}, z_\mathrm{o})$ are fixed parameters. The pick-and-place of random target and object positions are not addressed in this work but may be accomplished in the future through the use of vision or tactile feedback from the robot.

2.3 Controller Design and Tuning

Synthetic Nervous Systems. To control the soft grasper for pick-and-place manipulation tasks, we developed a bio-inspired neural network controller using the Synthetic Nervous System (SNS) approach. Synthetic Nervous Systems (Fig. 4A) are neural network models inspired by the biophysics of neurons [30, 31]. This approach treats synaptic inputs to a neuron as conductance changes while simplifying the function of the neuron's axon as a nonlinear relationship between the membrane potential and neural activity. This representation endows a model neural network with the necessary inductive bias to conduct nonlinear operations with low computational complexity [7, 11, 15]. The dynamics of the ith neuron in an SNS can be described as the following ordinary differential equations [31]:

$$C_{\mathrm{m},i}\frac{\mathrm{d}U_i}{\mathrm{d}t} = g_{\mathrm{m},i}(E_{\mathrm{r},i} - U_i) + \sum_j g_{ij}y_j(E_{ij} - U_i) + I_i \tag{1}$$

$$y_i = \phi_i(U_i) = \frac{\min(\max(U_i, E_{\mathrm{lo},i}), E_{\mathrm{hi},i})}{E_{\mathrm{hi},i} - E_{\mathrm{lo},i}} \tag{2}$$

where Eq. 2 represents a piecewise-linear relationship between membrane potential U_i and neural activity y_i, with $E_{\mathrm{lo},i}$ and $E_{\mathrm{hi},i}$ the lower and upper limit of the activation function ϕ_i, respectively. In Eq. 1, $C_{\mathrm{m},i}$, $g_{\mathrm{m},i}$, and $E_{\mathrm{r},i}$ are the membrane capacitance, leak conductance, and resting potential of the neuron, respectively. The summation term is the net synaptic current, where the product of maximal conductance of the jth synapse g_{ij} and the corresponding presynaptic neural activity y_j defines the synaptic conductance, and E_{ij} is the reversal potential of the synapse. I_i represents external stimuli or bias current.

After determining the specific network structure, the parameters in an SNS must be set appropriately to accomplish the assigned tasks of each pathway. The use of Functional Subnetworks (FSNs) [8, 31] is an analytical approach to

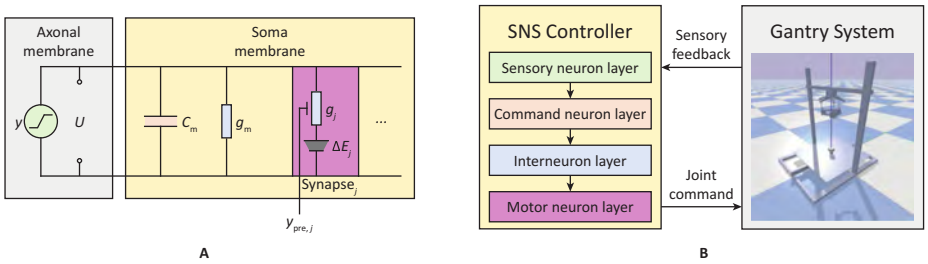

Fig. 4. A Schematic of non-spiking, single-compartment neurons in Synthetic Nervous Systems (U: membrane potential, y: neural activity, C_{m}: membrane capacitance, G_{m}: leak conductance, g: maximal synaptic conductance, ΔE: reversal potential, y_{pre}: presynaptic neural activity) and **B** a bio-inspired SNS controller for the pick-and-place control of the soft grasper. In SNSs, neurons are represented by single-compartment units with conductance-based inputs and rated outputs. All neurons in our neural network controller are modeled in the SNS framework. The hierarchical structure of the controller was inspired by the nervous system of *Aplysia*.

solving the parameter-tuning problem in SNSs. By deriving the constraints that govern the network behaviors, an SNS user can design static networks for elementary mathematical operations and dynamic networks for differentiation and integration. However, the analytical nature of FSNs limits their application in constructing complex networks and pathways implementing highly nonlinear operations. A more systematic way to tune the SNS parameters is using supervised learning methods. We can discretize Eq. 2 by a semi-implicit method [17] and express the governing differential equations of n neurons as a recurrent neural network (RNN) model in machine learning [18]

$$\hat{\boldsymbol{\tau}}_t = \frac{\boldsymbol{\tau}}{1 + \boldsymbol{V}\phi(\boldsymbol{h}_{t-1})} \tag{3}$$

$$\boldsymbol{z}_t = \frac{\Delta}{\hat{\boldsymbol{\tau}}_t + \Delta} \tag{4}$$

$$\hat{\boldsymbol{h}}_t = \frac{\boldsymbol{b} + \boldsymbol{W}\phi(\boldsymbol{h}_{t-1})}{1 + \boldsymbol{V}\phi(\boldsymbol{h}_{t-1})} \tag{5}$$

$$\boldsymbol{h}_t = (1 - \boldsymbol{z}_t) \odot \boldsymbol{h}_{t-1} + \boldsymbol{z}_t \odot \hat{\boldsymbol{h}}_t \tag{6}$$

where t is the current time and Δ is the time step. $\boldsymbol{h}_t$ denotes the state vector $[U_1, \cdots, U_n]^\top$. $\boldsymbol{z}_t$ and $\boldsymbol{h}_t$ are two intermediate variables defined in Eq. 4 and Eq. 5, respectively. $\boldsymbol{\tau} = [\tau_1, \cdots, \tau_n]^\top$ is the time constant vector with $\tau_i = C_{\mathrm{m},i}/g_{\mathrm{m},i}$ representing the time constant of ith neuron, while $\boldsymbol{\tau}_t$ defined in Eq. 3 is the effective time constant vector. The weight matrix $\boldsymbol{W} = (w_{ij})$ and conductance matrix $\boldsymbol{V} = (v_{ij})$ are two $n \times n$ matrices with $w_{ij} = g_{i,j}E_{ij}/g_{\mathrm{m},i}$ and $V_{ij} = g_{i,j}/g_{\mathrm{m},i}$ representing the normalized synaptic weight and synaptic conductance from the jth neuron to the ith neuron, respectively. $\odot$ denotes element-wise product. We can then formulate the parameter tuning problems of SNSs as machine learning tasks such as function approximation or time series prediction and adopt

methods like backpropagation through time (BPTT) [35] to effectively calculate the gradient and optimize the parameters $\boldsymbol{\tau}$, $\boldsymbol{W}$, $\boldsymbol{V}$, $\boldsymbol{E}_{\text{hi}}$, and $\boldsymbol{E}_{\text{lo}}$. Due to the conductance-based synapses, the activities of presynaptic neurons exist in both the numerator and denominator of Eq. 5. This rational function, as an additional source of nonlinear computation besides the activation function ϕ, increases the expressive power of SNSs [7], allowing users to design compact and interpretable controllers with sparse synaptic connections. In [18], it is demonstrated that compact SNSs have superior performance to classical neural network models such as multilayer perceptrons (MLPs) in terms of implementing nonlinear arithmetic operations that are essential for robotic control. Furthermore, bio-inspired neural network models can exploit the temporal nature of the task, enabling them to filter out transient disturbances and provide superior noise resiliency, compared to feedforward models [17].

An SNS Controller for the Soft Grasper. Using SNSs, we designed a soft grasper controller to implement pick-and-place manipulation. The structure of the neural network controller (Fig. 4B) was inspired by the nervous system of *Aplysia*. *Aplysia* can achieve robust and multifunctional feeding control based on a relatively small number of neurons [6,34]. Its command-like cerebral-buccal interneurons in the cerebral ganglion receive afferent feedback from sensory neurons. They coordinate behaviors by mediating the buccal interneurons in the buccal ganglion [12]. The buccal interneurons, in turn, mediate motor neurons to generate features that are fundamental for the selected feeding behavior [13]. Our grasper controller used a similar structure. The sensory neuron layer (Fig. 5A) received the grasper position $(x_{\text{g}}, y_{\text{g}}, z_{\text{g}})$, object position $(x_{\text{o}}, y_{\text{o}}, z_{\text{o}})$, target position $(x_{\text{t}}, y_{\text{t}}, z_{\text{t}})$, and contact force (F_1, F_2, F_3) between the three jaws and the object. [1] The output neurons of this layer detected whether the distance between the grasper and the object/target (Δo/Δt) was greater than a relatively large threshold ($\text{th}_1 = 8$ cm) or a relatively small threshold ($\text{th}_2 = 1$ cm). Two model neurons were included in the controller to detect whether a stable contact had been established (all forces were greater than a large threshold $\text{th}_{F,1} = 15$ N) or discarded (any force was greater than a small threshold $\text{th}_{F,1} = 0.5$ N). The command neuron layer (Fig. 5B) contained 8 neurons, each representing a critical behavior in the pick-and-place task. The excitation of a neuron led to the generation of the corresponding behavior. Synapses from the sensory layer ensured the behaviors could be executed in sequence. Neurons in the interneuron layer (Fig. 5C) were implemented with synaptic connections to motor neurons(Fig. 5D), which defined four necessary motion primitives in the pick-and-place control. By selectively exciting the interneurons, a command neuron can accomplish its behavioral coordination function. For example, the reaching-the-object command neuron excites the moving-to-the-object (Obj) interneuron. In contrast,

[1] Although we can achieve variable stiffness through active pressure control, we set the pressure applied to the soft jaws as a constant in this work. The regulation of the stiffness is treated as future work (see section 4)

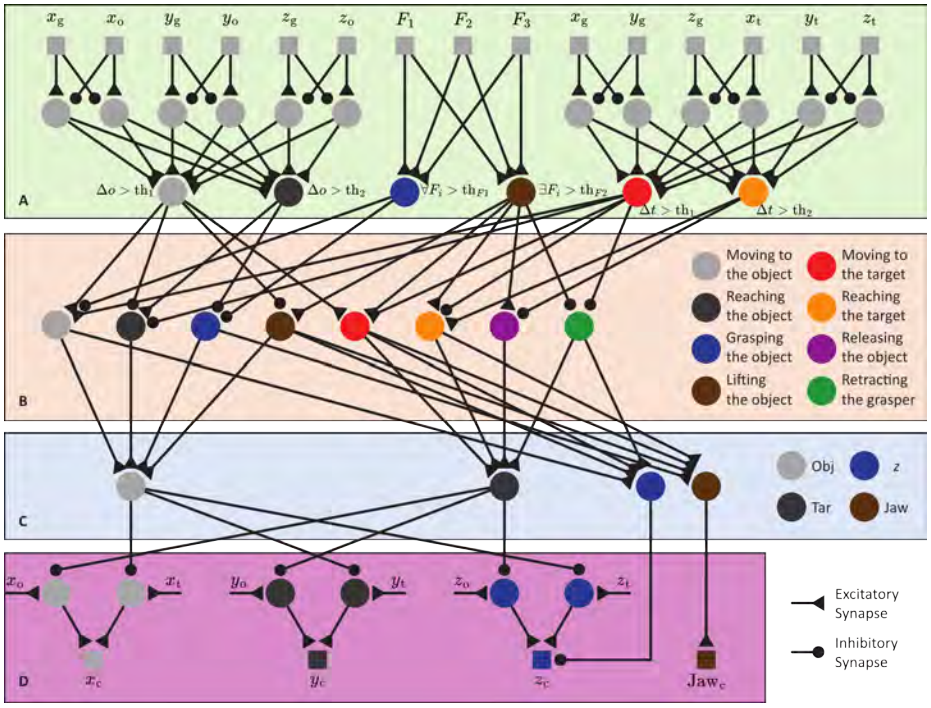

Fig. 5. A Neurons and synaptic connections in the sensory neuron layer, **B** command neuron layer, **C** interneuron layer, **D** and motor neuron layer of the soft grasper controller. Neurons in the interneuron layer represent four different motion primitives, namely moving to the object (Obj), moving to the target (Tar), lifting the grasper (Δz) up, and closing the jaw (Jaw). The activities of motor neurons represent the joint commands sent to the gantry system (grasper position (x_c, y_c, z_c) and radial contraction of the grasper Jaw_c). A command neuron will be activated if all of its excitatory neurons are firing while inhibitory neurons are silent. In contrast, an interneuron will be activated if any of its excitatory neurons are firing.

the reaching-the-target command neuron excites the moving-to-target (Tar) and closing-the-jaw (Jaw) interneurons.

To find appropriate parameters for the SNS controller, we built the neural network model in Pytorch (version 2.1.0, Python version 3.9.16) [23] and used the supervised learning paradigm introduced in the previous subsection 2.3 to train the controller in an offline and layer-wise manner. The learning was formulated as a time sequence prediction task. The training set for each layer contained 10000 training examples. Each training example included randomly sampled constant series as layer inputs and the desired layer outputs specified in Fig. 5 as label series. Specifications of the SNS training are summarized in Table 1.

Table 1. The training parameters of the soft grasper controller.

Training parameters	**Value**
Time step	0.1 sec
Number of training examples	10000
Window size	50
Batch size	200
Training epoch	50
Training method	BPTT
Optimizer	Adam
Performance	Mean squared error (MSE)

2.4 Testing SNS control on the Soft Grasper Platform

To demonstrate the effectiveness of the controller in performing a pick-and-place task with the soft grasper, the soft grasper was mounted to a customized gantry, and the pressure of the pneumatic components was controlled by a pressure regulator (Fig. 3). The gantry and the pressure regulator were previously presented in [18] and [5], respectively. The pressurization of the closure muscle and each of the three soft jaws was independently controlled by the pressure controller which received pressure commands from and sent pressure sensor readings to the host PC in real-time. Communication with both the pressure regulator and the gantry occurred over separate serial ports at 115200 Baud-rate.

In accordance with the controller tuned in simulation, at the start of a pick-and-place test, each of the jaws was inflated to a pressure of 1 psig. Once all the jaws were within 0.050 psig of this threshold, the inlet and outlet valves for the corresponding ports on the pressure regulator were kept closed for the duration of the experiment to maintain a constant volume of air within the jaws. The controller sent position commands for the x-y-z axes of the gantry and sent the pressure command corresponding to the desired radial change of the closure muscle to the pressure regulator. The pressure readings of the closure muscle and each of the soft jaws were reported by the pressure regulator and logged on the host PC. Changes in the measured pressure at each of the jaws were used as a

proxy for contact force measurement. For compatibility with the SNS controller thresholds, force feedback presented to the SNS was calculated as follows. The change in pressure (measured in psig) from the 1 psig setpoint was scaled by a factor of 5 if the difference was greater than 0.2 psig; otherwise, the force for that jaw was set to 0. The 0.2 psig threshold was manually tuned to prevent false triggering of a state change from sensor noise. The scale factor of 5 was manually tuned so that when secure contact with an object was initiated, it would trigger a change in state from Phase III (close grasper) to Phase IV (lift object).

3 Results and Discussion

3.1 Force vs. pressure characterization for soft jaw

The soft deformable jaws demonstrated increased reaction force as a function of both indentation distance and pressure applied to the internal cavity of the jaws (Fig. 6A). The following nonlinear empirical model was fitted to the data using MATLAB's `fitnlm` routine:

$$F_R[N] = (0.0416 + 0.505P_J^{1.0647})(0.179^{2P_J} l_d^2 + 0.891^{P_J} l_d + 5.4641) \quad (7)$$

where F_R is the reaction force in N, l_d is the indentation depth in mm and P_J is the pressure applied to the jaw in psig.

Similar to the increase in reaction force with increased pneumatic pressure applied to the jaw at a given indentation depth, there was also an increase in stiffness. This was reflected in the empirical model by differentiating F_R (Eq. 7) with respect to l_d:

$$k_{eff}[N/mm] = \frac{\partial F_R}{\partial l_d} = (0.0416 + 0.505P_J^{1.0647})(0.891^{P_J} + 0.3581^{2P_J} l_d) \quad (8)$$

where k_{eff} is the stiffness in N/mm.

At pressures beyond atmospheric (i.e. greater than 0 psig), there was a non-zero force present at 0 indentation depth. This was because the faces of the soft jaw bulged outward when pressurized. This increase in the effective size of the jaw has the potential benefit of allowing the grasping of smaller objects than was initially designed for by decreasing the radius of the space enclosed by the jaws when the closure muscle is fully activated (19.5 mm, Fig. 1). However, this increase in the size of the jaw was coupled with an increase in both force and stiffness and may not be appropriate in all grasping applications, particularly for very small and fragile objects. Future work will look at ways to limit the deflection of the jaw surface during inflation, such as using selective fiber reinforcements.

While the empirical model captures the change in contact force as a function of pressure and indentation depth, it does not capture the time-varying dynamics of the soft jaw. Including the dynamics introduced by the viscoelasticity of the

elastomeric materials and inflation of the soft jaw will be important for real-time control of the grasper's mechanical properties. Future work will characterize such dynamics through both experiment and simulation using finite-element-based methods.

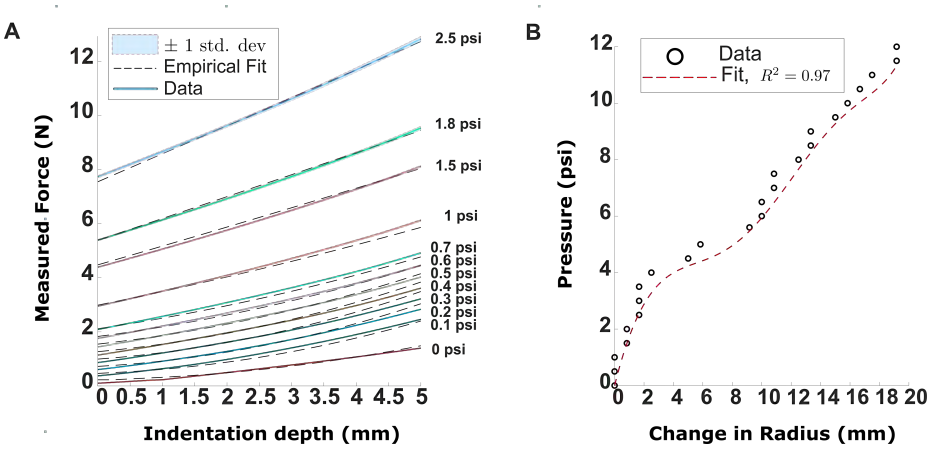

Fig. 6. A Reaction force and stiffness increase with increased pressure applied to the internal cavity of the jaw. Indentation depth was measured relative to the height of the jaw in the 0 psig state. **B** Pressure required to achieve a given change in the radius of the closure muscle. To achieve changes larger than a few mm, pressures beyond 5 psig were required. At 12 psig, the closure muscle reached the limit of its contraction.

3.2 Mapping input pressure to radial contraction in the closure muscle

The closure muscle showed a non-linearly monotonic decrease in radius as pressure was increased (Fig. 6B). The pressure required to achieve a given change in radius was captured by the following 6th-order polynomial fit to the data:

$$\begin{aligned} P_C[psig] =& 3.03 \times 10^{-6} \Delta r^6 - 1.26 \times 10^{-4} \Delta r^5 + 9.37 \times 10^{-4} \Delta r^4 \\ &+ 0.0217 \Delta r^3 - 0.364 \Delta r^2 + 2.075 \Delta r \end{aligned} \tag{9}$$

where P_C is the pressure applied to the closure muscle in psig and Δr is the decrease in radius in mm. Decreases in the radius from the uninflated closure muscle state are considered positive.

The closure muscle contracted only a few mm for pressures below 5 psig, with most of the contraction occurring between 5-11 psig. At pressures beyond 12 psi, there was no noticeable reduction in the radius of the grasper. This is consistent with the previously observed behavior of these types of McKibben

actuator rings [5], where although the inner latex bladder increases in diameter for pressures below 5 psig, it is not yet in contact with the over-expanded mesh, and so little contraction occurs. The maximum achievable decrease in radius of 19 mm was lower than the expected 27 mm. This may be caused by two factors: 1) the tubing used to connect the two McKibben actuators in the same layer of the closure muscle reduces the effective length of the McKibben and doesn't contribute to contraction, and 2) The rigid jaw supports that were sewn into the closure muscle served as constraints that prevented those regions from contracting. Future iterations of the soft grasper should attempt to mitigate these effects by fabricating the McKibben actuators out of a single long latex bladder and fabricating the entire jaw structure out of deformable materials that can compress circumferentially with the contraction of the closure muscle.

3.3 Controlling the pick-and-place grasper with an SNS in simulation

We first tested the effectiveness of the proposed SNS controller in the simulation environment. In the simulation, the soft grasper model could maintain sufficient contact with the object and successfully complete the task in response to the activity of the command neurons (Fig. 7).

While the simulation was able to modulate the change in contact stiffness with pressure based on the empirical model (Eq. 8), the simulation did not fully capture the physics of contact between the object and the soft jaws. The deformation of the soft jaws around the grasped object was not captured by the simulation because of the use of rigid bodies to represent the jaws. Future work will address the limitations of the current simulation environment by using finite element-based methods (FEA) to capture the physics of the interaction more accurately.

3.4 Controller validation on physical robot w/grasper

The controller tuned in the simulation environment was then used to control the physical gantry and soft robot (Fig. 3). To approximate the position control used in the simulation for use with the physical closure muscle, the experimentally determined relationship between change in radius and input pressure was used (Eq. 9). With no further tuning of the controller thresholds and appropriate scaling of the change in contact pressure of the jaw as a proxy for contact force, the grasper successfully executed all nine phases of SNS control (Fig. 8A). In addition, the grasper successfully completed the pick-and-place operation on a variety of different object shapes and masses, up to a maximum tested weight of 706 g (Fig. 8B). No additional tuning of the SNS controller was required to account for the different shapes and masses of the objects grasped.

While there was a potential risk of damage to the grasper or the grasped object because the dimensions of the object were not accounted for in the control, the compliance of the soft jaws and the closure muscle made it not likely to damage the objects grasped in this work. To grasp fragile objects in the future

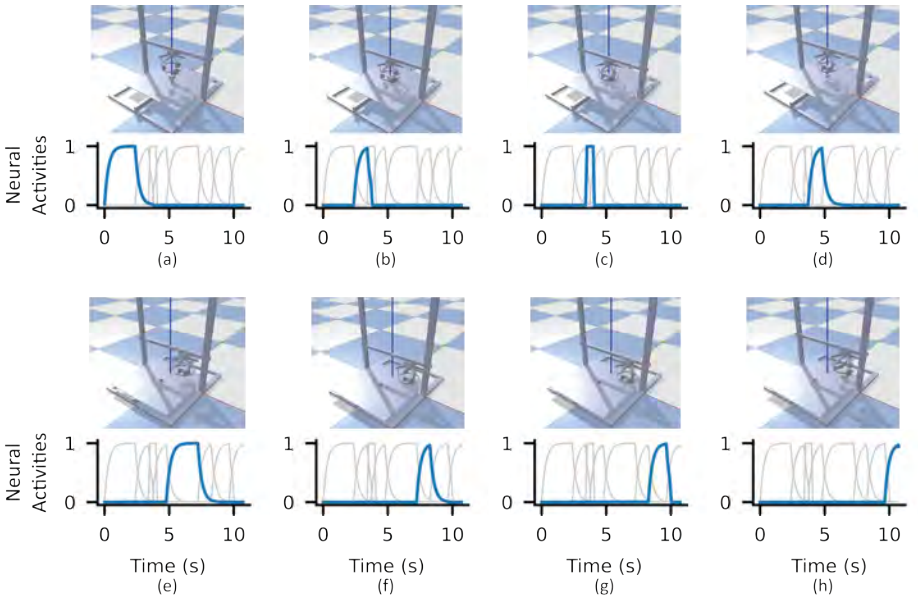

Fig. 7. Different phases of the pick-and-place manipulation and the activities of the working command neurons. The top figure represents the simulation environment and the bottom figure indicates the temporal activity of the command neuron from Fig. 5B that is active in that phase (bold blue line). **A** Moving to the object. **B** Reaching the object. **C** Grasping the object. **D** Lifting the object. **E** Moving to the target. **F** Reaching the target. **G** Releasing the object. **H** Retracting the grasper.

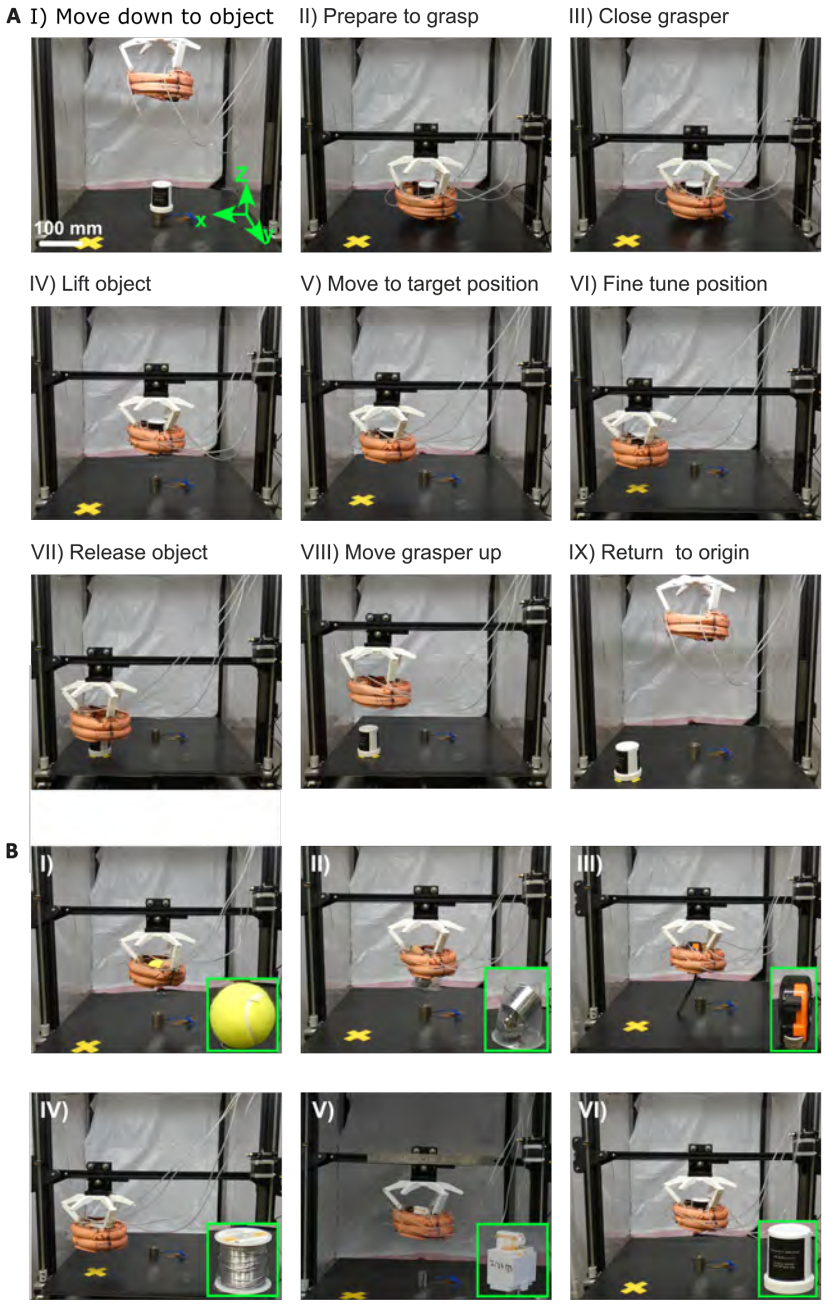

Fig. 8. A Phases of Grasper Motion. **B** Under SNS control, the grasper can successfully grasp and manipulate a wide range of common household and laboratory objects (Inset image shows objects). Masses of objects tested include I) 58 g, II) 706 g, III) 328 g, IV) 497 g, V) 62 g, VI) 62.9 g.

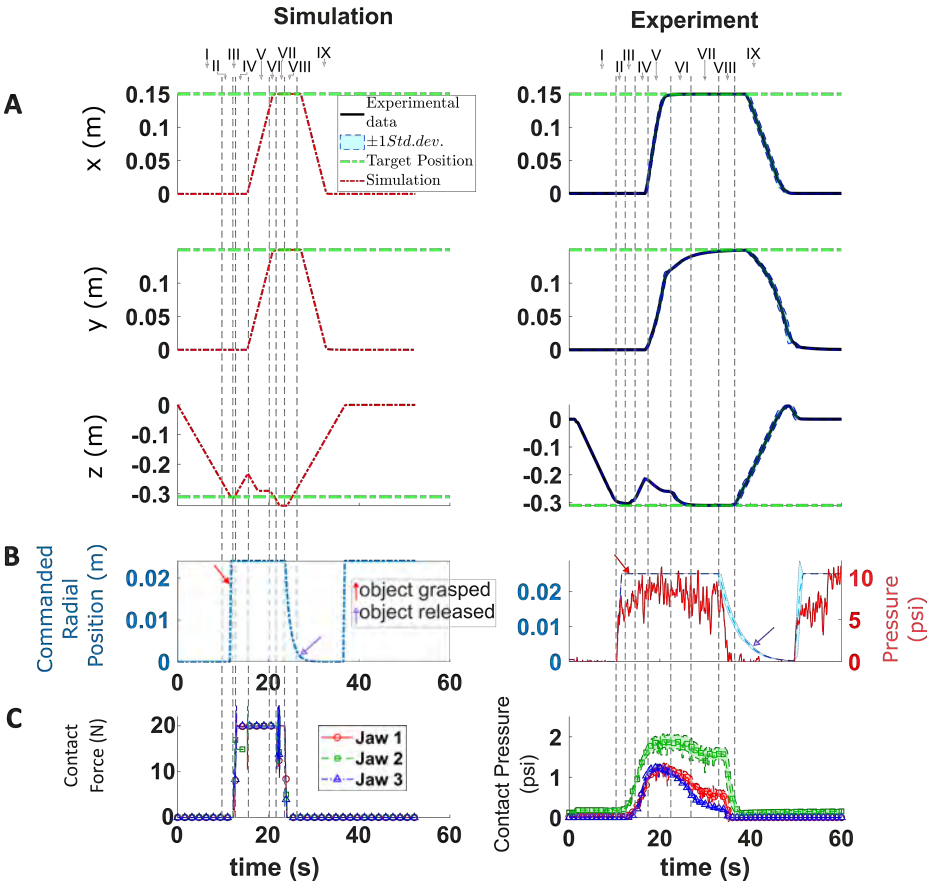

Fig. 9. A-C Comparison of simulation (left) vs. experimental (right) kinematics, pressures, and forces. All data shown were from three pick-and-place trials of object VI in Fig. 8. **A** Kinematics of the grasper position in the x, y and z axes. Phases of the SNS control (I through IX) are indicated at the top. The kinematics of the actual robotics system followed a similar shape to the experimental protocol but took longer to execute phases VI-IX. **B** Commanded radial position. In the physical grasper, the measured pressure (right) followed the general trend of the commanded radial position. **C** Pressure increased upon making contact with the object (right), which corresponds to the increased contact force seen in simulation (Phases III-IV). Pressure decreased in the jaws when the object was released (Phases VII-IX).

however, it will be important to actively control the radial opening of the grasper to enclose the object without damaging it by providing feedback of shape information. Methods for achieving such feedback include vision-based methods, or processing the spatial contact information provided by the change of pressure in each of the jaws. Currently, the controller does not reason about the change in pressure in each jaw individually to extract shape information about the object, but this could be explored in the future. As the internal radius of the closure muscle is on the order of centimeters (design target: 19 mm, measured: 27 mm) when fully inflated, the grasper was incapable of grasping very thin objects. In contrast, *Aplysia* excels at tearing and ingesting thin objects such as seaweed using the closure of the feeding apparatus' internal grasper that can protract to grasp the seaweed and retract to ingest the seaweed [14]. Future versions of this bio-inspired soft grasper will incorporate similar structures to grasp a larger range of objects.

The physical robotic system replicated key features of the dynamics of the SNS-controlled simulation (Fig. 9A-C). The pressurization of the grasper (Fig. 9B right plot) began when the commanded radial position increased at the start of Phase III (Close Grasper). The transition from Phase III to Phase IV (Lift Object) corresponded to an increase in contact pressure in all three jaws as the grasper closed around the object (Fig. 9C). When the object was released in Phase VII and the grasper began to move up in Phase VIII, there was a corresponding decrease in contact pressure that tracked with the decrease in contact force seen in the simulation (Fig. 9C). The kinematics of the gantry to which the grasper was attached also demonstrated qualitatively similar behavior to the simulation (Fig. 9A), which aligns with our prior observations of transferring SNS-controllers of the gantry from simulation to the physical platform [18].

While the grasper was able to execute each phase of the pick-and-place task successfully, it should be noted that there were deviations in the physical grasper robot's dynamics when compared to the expected simulation results. The physical gantry robot took 51.2 s to complete the pick-and-place task compared to 37.1 s in the simulation. A large portion of this discrepancy was due to phases VII-VIII, where the gantry moved very slowly as it approached its target so as not to overshoot it. In the physical gantry robot, hardware and communication limitations prevented rapid fine-tuning of position [18].

Another noticeable difference between the simulation and the physical robot was seen when grasping smaller objects, where the grasper attempted to lift (Phase IV) before the grasper's closure muscle had completely pressurized. This was likely because the simulation did not incorporate the dynamics of the closure muscle's inflation (and deflation) and assumed the closure muscle could respond instantaneously to a position command. This was likewise reflected when attempting to release the object (Phase VII). During object release, the grasper incompletely depressurized before lifting (Phase VIII), causing the object to lift slightly before dropping to the platform. This increased time to create contact (Phase II-Phase IV) and lose contact (Phase VII-Phase VIII) with the grasped object was reflected in the different rise times of the contact force in the sim-

ulation compared to the contact pressure in the physical grasper robot (Fig. 9C). Including the dynamics of both the jaw inflation and the closure muscle in the simulation will allow us to tune the SNS controller to account for these dynamics and achieve better pick-and-place performance in the future. The gap between the simulation and the physical grasper can be further minimized by incorporating online learning of the parameters of the SNS. While the controller operated in real-time as the transition from one phase to another was dependent on position and force feedback from the physical robot (Fig. 5), the parameters of the SNS were learned offline. Future work will explore such online methods for learning and tuning the SNS parameters.

It was also observed that there was asymmetry in the contact pressures measured in the three jaws, which was not exhibited in the contact forces in the simulation (Fig. 9C). While two of the jaws showed similar pressure changes, the third jaw exhibited about 0.4 psig higher pressure. This asymmetry may be attributed to the misalignment of the grasper relative to the gantry or the misalignment of the center of the object relative to the center of the grasper. Future iterations of the grasper will replace the tilt attachments (Fig. 1A), which are currently 3D printed, with McKibben actuators to allow active tilting of the closure muscle, which may lead to more even contact pressure distributions.

4 Conclusions

In this work, we have demonstrated that an SNS-controlled *Aplysia*-inspired soft robot grasper can successfully pick-and-place objects of varying mass and size (Fig. 8). Inspired by *Aplysia*'s ability to modulate grasp force and conform to the shape of the grasped object, we presented the design and manufacture of a SNS-controlled soft grasper capable of closing around the target object. The grasper successfully modulated contact stiffness while providing simultaneous feedback of contact using pneumatic soft actuators (Fig. 1). To our knowledge, this is the first time the Synthetic Nervous System approach has been adapted for soft robotic grasping and manipulation.

Future work will aim to expand the adaptability of the soft grasping platform by improving the physical grasper, controller and simulation. To improve the fidelity of the simulation to the physical robot, the temporal dynamics of the closure muscles and the soft jaws will be included in the simulation. In addition, the positions of the object and target locations are currently fixed and the parameters of the SNS are tuned offline. To improve the flexibility of the grasper robot, future work will explore real-time feedback of the object and target position and online methods for learning the SNS parameters at run-time. The tunable stiffness of the soft jaws was not exploited during the pick-and-place tasks. Future work will explore the benefits of tunable stiffness to real-time manipulation tasks, particularly for soft and fragile objects.

The ability of this soft grasper platform to successfully manipulate objects of variable size and mass in real-time with limited tuning of the controller is exciting because it demonstrates that a soft grasper can combine the benefits of

compliant surfaces inherent to soft robotic graspers with the efficient and robust computational advantages of the SNS. In addition, the SNS is capable of emergent dynamics that we will continue to explore in future work. For instance, in limited trials, it was observed in both simulations and on the physical grasper that the SNS controller had the ability to correct some grasping mistakes. Further development of the platform will attempt to exploit this emergent feature for use in the robust grasping of fragile and slippery objects, which may be particularly important in agricultural and industrial applications.

Acknowledgements The authors would like to thank Ashlee Liao, Saul Schaffer, and Avery Williamson for their helpful comments in editing this manuscript.

References

1. Becker, K., Teeple, C., Charles, N., Jung, Y., Baum, D., Weaver, J.C., Mahadevan, L., Wood, R.: Active entanglement enables stochastic, topological grasping. Proceedings of the National Academy of Sciences **119**(42) (Oct 2022)
2. Ciocarlie, M., Miller, A., Allen, P.: Grasp analysis using deformable fingers. In: 2005 IEEE/RSJ International Conference on Intelligent Robots and Systems. pp. 4122–4128 (Aug 2005), iSSN: 2153-0866
3. Coulson, R., Stabile, C.J., Turner, K.T., Majidi, C.: Versatile Soft Robot Gripper Enabled by Stiffness and Adhesion Tuning via Thermoplastic Composite. Soft Robotics **9**(2), 189–200 (Apr 2022)
4. Coumans, E., Bai, Y.: Pybullet, a python module for physics simulation for games, robotics and machine learning (2016)
5. Dai, K., Sukhnandan, R., Bennington, M., Whirley, K., Bao, R., Li, L., Gill, J.P., Chiel, H.J., Webster-Wood, V.A.: SLUGBOT, an Aplysia-Inspired Robotic Grasper for Studying Control. In: Hunt, A., Vouloutsi, V., Moses, K., Quinn, R., Mura, A., Prescott, T., Verschure, P.F.M.J. (eds.) Biomimetic and Biohybrid Systems. pp. 182–194. Lecture Notes in Computer Science, Springer International Publishing, Cham (2022)
6. Gill, J.P., Chiel, H.J.: Rapid Adaptation to Changing Mechanical Load by Ordered Recruitment of Identified Motor Neurons. eNeuro **7**(3) (2020)
7. Hasani, R., Lechner, M., Amini, A., Rus, D., Grosu, R.: Liquid time-constant networks. In: Proceedings of the AAAI Conference on Artificial Intelligence. vol. 35, pp. 7657–7666 (2021)
8. Hilts, W.W., Szczecinski, N.S., Quinn, R.D., Hunt, A.J.: A dynamic neural network designed using analytical methods produces dynamic control properties similar to an analogous classical controller. IEEE Control Systems Letters **3**(2), 320–325 (2018)
9. Hunt, A., Szczecinski, N., Quinn, R.: Development and Training of a Neural Controller for Hind Leg Walking in a Dog Robot. Frontiers in Neurorobotics **11** (2017)
10. Hurwitz, I., Susswein, A.J.: Adaptation of Feeding Sequences in *Aplysia Oculifera* to Changes in the Load and Width of Food. Journal of Experimental Biology **166**(1), 215–235 (May 1992)
11. Jayakumar, S.M., Czarnecki, W.M., Menick, J., Schwarz, J., Rae, J.W., Osindero, S., Teh, Y.W., Harley, T., Pascanu, R.: Multiplicative interactions and where to find them. In: 8th International Conference on Learning Representations, ICLR 2020, Addis Ababa, Ethiopia, April 26-30, 2020. OpenReview.net (2020)

12. Jing, J., Weiss, K.R.: Neural Mechanisms of Motor Program Switching in *Aplysia*. The Journal of Neuroscience **21**(18), 7349–7362 (Sep 2001)
13. Jing, J., Weiss, K.R.: Generation of variants of a motor act in a modular and hierarchical motor network. Current Biology **15**(19), 1712–1721 (2005)
14. Kehl, C.E., Wu, J., Lu, S., Neustadter, D.M., Drushel, R.F., Smoldt, R.K., Chiel, H.J.: Soft-surface grasping: radular opening in *Aplysia californica*. J. Exp. Biol. **222**(16) (2019)
15. Koch, C.: Biophysics of Computation: Information Processing in Single Neurons . Oxford University Press (Nov 1998)
16. Kuppuswamy, N., Alspach, A., Uttamchandani, A., Creasey, S., Ikeda, T., Tedrake, R.: Soft-bubble grippers for robust and perceptive manipulation. In: 2020 IEEE/RSJ International Conference on Intelligent Robots and Systems (IROS). pp. 9917–9924 (2020)
17. Lechner, M., Hasani, R., Amini, A., Henzinger, T.A., Rus, D., Grosu, R.: Neural circuit policies enabling auditable autonomy. Nature Machine Intelligence **2**(10), 642–652 (2020)
18. Li, Y., Sukhnandan, R., Gill, J.P., Chiel, H.J., Webster-Wood, V., Quinn, R.D.: A Bioinspired Synthetic Nervous System Controller for Pick-and-Place Manipulation. arXiv (May 2023). , arXiv:2305.10954
19. Lynch, K.M., Park, F.C.: Modern robotics: mechanics, planning, and control. Cambridge university press, Cambridge (2017)
20. Majidi, C.: Soft-Matter Engineering for Soft Robotics. Advanced Materials Technologies **4**(2), 1800477 (2019)
21. Mangan, E.V., Kingsley, D.A., Quinn, R.D., Sutton, G.P., Mansour, J.M., Chiel, H.J.: A biologically inspired gripping device. Ind. Robot **32**(1), 49–54 (2005)
22. Nishimura, T., Suzuki, Y., Tsuji, T., Watanabe, T.: Fluid Pressure Monitoring-Based Strategy for Delicate Grasping of Fragile Objects by A Robotic Hand with Fluid Fingertips. Sensors (Basel, Switzerland) **19**(4), 782 (Feb 2019)
23. Paszke, A., Gross, S., Massa, F., Lerer, A., Bradbury, J., Chanan, G., Killeen, T., Lin, Z., Gimelshein, N., Antiga, L., Desmaison, A., Kopf, A., Yang, E., DeVito, Z., Raison, M., Tejani, A., Chilamkurthy, S., Steiner, B., Fang, L., Bai, J., Chintala, S.: Pytorch: An imperative style, high-performance deep learning library. In: Advances in Neural Information Processing Systems 32, pp. 8024–8035. Curran Associates, Inc. (2019)
24. Peters, J., Nolan, E., Wiese, M., Miodownik, M., Spurgeon, S., Arezzo, A., Raatz, A., Wurdemann, H.A.: Actuation and stiffening in fluid-driven soft robots using low-melting-point material. In: 2019 IEEE/RSJ International Conference on Intelligent Robots and Systems (IROS). pp. 4692–4698. IEEE, Macau, China (Nov 2019)
25. Root, S.E., Preston, D.J., Feifke, G.O., Wallace, H., Alcoran, R.M., Nemitz, M.P., Tracz, J.A., Whitesides, G.M.: Bio-inspired design of soft mechanisms using a toroidal hydrostat. Cell Reports Physical Science **2**(9), 100572 (Sep 2021)
26. Roth, F.L., Driscoll, R.L., Holt, W.L.: Frictional Properties of Rubber. Rubber Chemistry and Technology **16**(1), 155–177 (03 1943). ,
27. Shintake, J., Cacucciolo, V., Floreano, D., Shea, H.: Soft Robotic Grippers. Advanced Materials **30**(29), 1707035 (2018)
28. Shintake, J., Schubert, B., Rosset, S., Shea, H., Floreano, D.: Variable stiffness actuator for soft robotics using dielectric elastomer and low-melting-point alloy. In: 2015 IEEE/RSJ International Conference on Intelligent Robots and Systems (IROS). pp. 1097–1102 (Sep 2015)

29. Suh, H.T., Kuppuswamy, N., Pang, T., Mitiguy, P., Alspach, A., Tedrake, R.: Seed: Series elastic end effectors in 6d for visuotactile tool use. In: 2022 IEEE/RSJ International Conference on Intelligent Robots and Systems (IROS). pp. 4684–4691 (2022)
30. Szczecinski, N.S., Hunt, A.J., Quinn, R.D.: Design process and tools for dynamic neuromechanical models and robot controllers. Biological cybernetics **111**(1), 105–127 (2017)
31. Szczecinski, N.S., Hunt, A.J., Quinn, R.D.: A functional subnetwork approach to designing synthetic nervous systems that control legged robot locomotion. Frontiers in neurorobotics **11**, 37 (2017)
32. Szczecinski, N.S., Quinn, R.D.: Template for the neural control of directed stepping generalized to all legs of MantisBot. Bioinspiration & Biomimetics **12**(4), 045001 (Jun 2017)
33. Wang, J., Chortos, A.: Control Strategies for Soft Robot Systems. Advanced Intelligent Systems **4**(5), 2100165 (2022)
34. Webster-wood, V.A., Gill, J.P., Thomas, P.J., Chiel, H.J.: Control for multifunctionality : bioinspired control based on feeding in *Aplysia californica*. Biol. Cybern. **114**(6), 557–588 (2020)
35. Werbos, P.: Backpropagation through time: what it does and how to do it. Proceedings of the IEEE **78**(10), 1550–1560 (1990)
36. Yoder, Z., Macari, D., Kleinwaks, G., Schmidt, I., Acome, E., Keplinger, C.: A soft, fast and versatile electrohydraulic gripper with capacitive object size detection. Advanced Functional Materials **33**(3), 2209080 (Nov 2022)
37. Zhang, B., Xie, Y., Zhou, J., Wang, K., Zhang, Z.: State-of-the-art robotic grippers, grasping and control strategies, as well as their applications in agricultural robots: A review. Computers and Electronics in Agriculture **177**, 105694 (Oct 2020)